Flexible inorganic-organic hybrids with dual inorganic components

Fan, Wei; Jensen, Lars Rosgaard; Ceccato, Marcel; Sørensen Quaade, Thomas; Gurevich, Leonid; Yu, Donghong; Smedskjær, Morten Mattrup

Published in:
Materials Today Chemistry

DOI (link to publication from Publisher):
10.1016/j.mtchem.2021.100584

Publication date:
2021

Document Version
Publisher's PDF, also known as Version of record

Materials Today Chemistry 22 (2021) 100584

Contents lists available at ScienceDirect

Materials Today Chemistry

journal homepage: www.journals.elsevier.com/materials-today-chemistry/

Flexible inorganic–organic hybrids with dual inorganic components

W. Fan [a], L.R. Jensen [b], M. Ceccato [c], T.S. Quaade [b], L. Gurevich [b], D. Yu [a, **], M.M. Smedskjaer [a, *]

[a] Department of Chemistry and Bioscience, Aalborg University, 9220 Aalborg, Denmark
[b] Department of Materials and Production, Aalborg University, 9220 Aalborg, Denmark
[c] Interdisciplinary Nanoscience Center (iNANO) and Department of Biological and Chemical Engineering, Aarhus University, 8200 Aarhus N, Denmark

ARTICLE INFO

Article history:
Received 3 June 2021
Received in revised form
18 August 2021
Accepted 6 September 2021
Available online xxx

Keywords:
Hybrid materials
Interpenetrating networks
Mechanical properties
Structure–property relations

ABSTRACT

Combining multiple inorganic components is an effective approach to improve the mechanical properties of inorganic–organic hybrid materials. The inorganic components can form interactions with the organic polymer matrix, and there is thus a need to understand the reinforcement mechanism under the optimal combination of organic polymer and inorganic particles. In this work, we prepared a series of dual inorganic particle–based titania/silica–poly(tetrahydrofuran)–poly(ε-caprolactone) (TiO_2/SiO_2–PTHF–PCL) hybrids by means of simultaneous cationic ring-opening polymerization and sol–gel reaction. In addition to constructing hybrid networks, the SiO_2 and TiO_2 components play important roles in multiple toughening mechanisms. The prepared dual inorganic hybrids feature enhanced thermal stability and mechanical properties when compared with the ones with a single inorganic component. The optimized mixing of such two inorganic components is identified through mechanical tests, revealing that the hybrid polymer$_{70}$/$(Si_{0.6}Ti_{0.4})_{30}$ (70/18/12 mass ratio) has the highest compressive failure strain (80%) and compressive ultimate strength (1.3 MPa) as well as storage modulus (120 kPa), enabling elongation of up to 37% when compared with its original length. We thus find that the dual inorganic component approach is an effective strategy to enhance the mechanical properties of hybrid materials, suggesting potential applications as scaffolds for tissue engineering and soft robotics.

1. Introduction

Designing and preparing mechanically tough, strong, and flexible materials is of great interest because such materials can find a broad range of applications from cartilage replacement and tissue engineering to soft robotics [1–3]. To this end, a potential strategy is to combine—at a nanometer scale—stiff inorganic glass networks with flexible organic polymer chains, which has been found as an effective strategy for enabling materials with both high strength and desirable flexibility [4–7]. We refer to such covalently linked inorganic–organic networks as hybrid materials, which could potentially inherit the advantages of both material families, including improved mechanical properties [7,8]. To enable this, the formation of covalent bonds between the inorganic and organic components is required, for further avoiding inorganic particle aggregation and improving the mechanical properties of such hybrid materials [8–12]. Hybrids with inorganic/organic interpenetrating networks (IPNs) have shown both high toughness and flexibility [12–17].

To ensure that covalent bonds between the inorganic and organic constituents are formed at the molecular level, synthesis routes based on *in situ* polymerization of organic monomers with a coupling agent have been applied. Monomers and coupling agents should be chosen based on their polymerization mechanism. For example, Jones et al. [12,18,19] applied a tetrahydrofuran (THF) monomer with a (3-glycidoxypropyl)trimethoxysilane (GPTMS) coupling agent as they undergo similar ring-opening processes. Xie et al. [20–23] chose to combine the acrylamide monomer with vinyltriethoxysilane as a coupling agent and thus take advantage of the common free-radical reactions of their vinyl groups. For constructing hybrid networks, the sol–gel method has been the most successful one as it forms hybrid IPNs during a long-time condensation process. Recent studies have shown that both density and Young's modulus of such hybrids can be controlled by changing the weight ratio of inorganic and polymer components [24].

* Corresponding author.
** Corresponding author.
E-mail addresses: yu@bio.aau.dk (D. Yu), mos@bio.aau.dk (M.M. Smedskjaer).

https://doi.org/10.1016/j.mtchem.2021.100584

Methods based on nanocomposite reinforcement [25,26], ionic bonding [27], and hydrogen bonding [28] have previously been explored to tailor the mechanical properties of hybrids. Among these, nanoparticle reinforcement could efficiently promote mechanical properties of materials, becoming the most commonly used method [27,28]. Insulating silica (SiO_2) nanoparticles [29] as well as semiconducting nanoparticles such as TiO_2 [25,26,30], SnO_2 [31], and ZrO_2 [32] have been applied as multifunctional cross-linkers in hybrids with improved mechanical properties in previous reports. Under the deformation process, intermolecular interactions (such as hydrogen bonds, London forces, and dipole−dipole interactions among polymer chains) dynamically break and recombine to homogenize hybrids. Polymer chains, which function as a transfer center, could dissipate energy and homogenize stress distribution during the stretching and compression process [20]. Inorganic particles, formed during the sol−gel process, not only function as an important component in constructing the IPN but also act as chemical/physical cross-linkers. Based on research of dual nanocomposites, multihierarchical inorganic nanoparticles could greatly improve the toughness of hybrids [33,34], which is achieved through multi-interactions of dual inorganic hierarchical nanoparticles with the polymer matrix [33–35] opposite to single-nanoparticle−based hybrids.

In this work, we designed and prepared a series of dual inorganic particle−based hybrids (DIHs), namely, titania/silica−poly(tetrahydrofuran)−poly(ε-caprolactone) (TiO_2/SiO_2−PTHF−PCL), to prepare inorganic−organic hybrids with improved fracture resistance and to further investigate the role of different inorganic components on the mechanical properties. The TiO_2/SiO_2−PTHF−PCL−based hybrids exhibited higher thermal stability and improved ultimate strength and failure strain than the single-nanoparticle−based hybrids. We performed *in situ* initiation of THF polymerization by GPTMS to ensure covalent linkage between the inorganic component and organic chains at the molecular level, whereas the IPN structure was controlled by adjusting the molar ratio between the two inorganic particles of SiO_2 and TiO_2. We found optimized mechanical properties of the DIH with its composition of 70/18/12 (mass ratio) for polymer/TiO_2/SiO_2. The obtained flexible hybrids could possibly find applications for soft devices as substitutes for load-bearing tissue.

2. Materials and methods

2.1. Materials

Polycaprolactone diol (HO−PCL−OH, Mn of 530 Da), $NaHCO_3$, KBr, 2,2,6,6-tetramethyl-1-piperidinyloxy (TEMPO), CH_3CN, THF, GPTMS, boron trifluoride−diethyl ether ($BF_3{\cdot}OEt_2$), tetraethylorthosilicate (TEOS), tetrabutyl orthotitanate (TBOT), triethanolamine (TEOA), and HCl (36 wt%) were all purchased from Sigma-Aldrich and used as received.

2.2. Synthesis of inorganic sol

For the silica-based sol, we initially prepared a solution of TEOS, deionized water, and 36 wt% hydrochloric acid (12 M HCl) with the molar ratio of 1:3.6:0.01. Then, the mixture was stirred vigorously to induce hydrolysis of TEOS. The completion of the reaction was confirmed when the mixture turned from cloudy to clear. The structure of silica is illustrated in Fig. S1. For the titanium-based sol, we firstly mixed TBOT and TEOA for 30 min at the molar ratio of 1:2. Then, an appropriate amount of deionized water was added into the TBOT/TEOA solution for achieving a Ti concentration of 1.25 mol/L, and finally, it was stirred for 2 h to achieve its sol.

2.3. Synthesis of organic sol

The method for synthesizing the organic precursor was based on the work of Jones and Tallia et al. [18]. To this end, HOOC−PCL−COOH was firstly prepared via following the existing method of oxidation of HO−PCL−OH by using TEMPO [17]. Second, 0.5 mol of the product was dissolved in anhydrous THF (at a concentration of 50 mg/mL). Third, 1 mol GPTMS was added. After continuously stirring for 30 min, 0.25 mol $BF_3{\cdot}OEt_2$ was added into the mixture to catalyze the epoxide ring-opening polymerization. This solution was stirred for 1.5 h for reaction. Then, the carboxylic acid groups in HOOC−PCL−COOH terminated the chain growth and formed the structure of GPTMS−PTHF−PCL.

2.4 Synthesis of hybrids

The inorganic silica-based sol and titania-based sol were added dropwise into the organic sol under different ratios as shown in Table S1 and stirred for 30 min at room temperature to obtain a homogeneous solution. Here, all the hybrids followed the weight ratio of (TEOS + TBOT)/PCL = 3/7, the molar ratio of TEOS: H_2O = 3.6:1 (the Si^{4+} concentration was 1.17 mol/L, and the hydrolyzed Ti^{4+} concentration was maintained at 1.25 mol/L), and the molar ratios of TEOS to TBOT were varied from 100/0, 80/20, 60/40, 40/60, 20/80, and 0/100, respectively (Table S1). Then, the mixed sol was transferred into cylindrical polytetrafluoroethylene molds, which were sealed for aging for 1 week at 40 °C. The lids were opened gradually to allow drying for the following three weeks at this temperature, and disc-shaped samples could then be recovered from the molds and used for characterization. The dimensions of the mold and the samples were $\Phi = 4.5$ and 4 cm, respectively, with an observed shrinkage of the sample on drying of about 21%. All samples are immersed in distilled water for 5 min to remove by-products and non-covalently bonded inorganic particles.

2.5. Structure characterization

Fourier-transform infrared (FTIR) spectroscopy was performed to determine the functional groups in inorganic bulks and hybrids by using a Bruker TENSOR II spectrometer along with Bruker Platinum attenuated total reflectance attachment, in the range of 4,000 to 400 cm^{-1}. All spectra were compiled from 64 consecutive scans and were baseline corrected using the vendor-supplied software OPUS. The surface morphology and element distribution in hybrids were tested by scanning electron microscopy (SEM) using a Zeiss Gemini SEM 500 instrument at 5 kV/10 μA. The size of TEOS and TBOT precursors was determined based on dynamic light scattering (DLS) measurements using a Zetasizer nano series (Malvern). Transmission electron microscopy (TEM) and high-angle annular dark-field scanning electron transmission microscopy (HAADF-STEM) images were obtained using a transmission electron microscope (TALOS F200X, FEI Company, USA) equipped with a TWIN lens system, an X-FEG electron source, and a CETA 16 M camera. The accelerating voltage was set to 200 kV. Elemental analysis was performed by energy-dispersive X-ray spectroscopy mapping recorded in STEM mode, whereas bright-field images were collected in TEM mode. The hybrid materials were carefully scraped off with a scalpel and then uniformly dispersed in absolute acetone using ultrasonication for 30 min.

The final inorganic vs. organic (I/O) weight ratio in the hybrids was determined by thermal gravimetric analysis (TGA) on an STA 449C (Netzsch) instrument. The samples were cut into small pieces and heated under a flow of air at the rate of 10 °C/min, from room temperature to 800 °C. The recorded weight loss could be ascribed to the combustion of the organic phase. To confirm the non-

crystalline structure of the hybrid materials, X-ray diffraction (XRD) analysis was carried out on pulverized samples at 2θ angles from 5° to 80° using a Panalytical Empyrean diffractometer with the Cu-Kα radiation source and Ni-filter. Atomic force microscopy (AFM) measurements were performed with an NTEGRA Aura AFM (NT-MDT, Russia) operating in tapping mode using HA_HR (ScanSens, Germany) cantilevers.

2.6. Mechanical tests of hybrids

Compression tests were performed using a Zwick Z100 universal testing machine equipped with a 100 kN load cell at room temperature. Samples were punched into cylinders with a diameter of 10 mm and a height of 5 mm. The crosshead speed was set to 1 mm/min. Tensile tests were performed using a Linkam TST350 tensile testing stage equipped with a 200 N load cell at room temperature. The hybrid samples were cut into rectangular shapes with a length of 30 mm, a width of 10 mm, and a thickness of 2 mm, and the crosshead speed was set to 2 mm/min. Dynamic mechanical analysis (DMA) was carried out using TA Instruments DMA 850. The DMA experiments were performed at room temperature in compression mode with an amplitude of 20 μm and a frequency in the range of 0.01–100 Hz.

3. Results and discussion

3.1. Hybrid synthesis and structure

Based on the previous work [18,35], the expected structures of the prepared DIHs (TiO_2/SiO_2–PTHF–PCL) are schematically illustrated in Fig. 1. GPTMS initiated the ring-opening process of THF and then covalently linked the polymer chains and inorganic components after adding inorganic precursors. The reaction mechanism is shown in Fig. S2 [18]. In addition, HOOC–PCL–COOH controlled the THF ring-opening reaction rate, ended the chain growth, and also formed strong intermolecular interactions, e.g. hydrogen bonds, with TiO_2/SiO_2 inorganic particles [18,35]. Experimentally we have found that the polymerization rate would be very fast and out of control when adding HOOC–PCL–COOH in the late stage of the chain propagation. Combining literature reports, we speculate that the rate of initiation of GPTMS by $BF_3 \cdot OEt_2$ would be strongly retarded by HOOC–PCL–COOH because of Lewis acid–base reactions between them [18], whereas the termination of the propagating chain would occur when boric-acid salts (formed between $BF_3 \cdot OEt_2$ and HOOC–PCL–COOH) would have been accumulated at a sufficiently high concentration, i.e. after a certain time of polymerization. Such a design achieves both covalent bonding between inorganic particles and polymer chains and non-covalent interactions (such as hydrogen bonds and London forces) in the hybrid system, which contributes to the improved mechanical properties in multiple ways. Covalent Si–O–Ti bonds are formed between TiO_2 and SiO_2 inorganic particles during the sol–gel condensation [35]. For the deformation processes, the intermolecular interactions, e.g. hydrogen bonds, are expected to break first, and then, covalent bonds break irreversibly at the final stage. In addition, it is known that the hydrogen bonds of PCL–COOH can trigger the self-healing ability of such hybrid materials [20,35], which is not expected to be affected by the titania incorporation in the present study. Multiple strengthening mechanisms in this system by dual inorganic components could effectively enhance the interactions among the various components in the hybrid networks and efficiently impede the fracture process during the material deformation. To systematically investigate how different inorganic components affect structures and mechanical properties of hybrids, we have compared six hybrids with different TiO_2 and SiO_2 compositions (see Table S1).

3.2. Structure confirmation of hybrids

An image of the hybrid polymer$_{70}$/(Si$_{0.6}$Ti$_{0.4}$)$_{30}$ sample is shown in Fig. 2a, revealing that this hybrid material possesses observable flexibility and can be bent to a large extent without breaking or permanently deforming. One may notice the lack of transparency for this hybrid sample (polymer$_{70}$/(Si$_{0.6}$Ti$_{0.4}$)$_{30}$), which could be ascribed to the TiO_2 nanoparticles (as further discussed in the following), because hybrid polymer$_{70}$/(Si$_1$Ti$_0$)$_{30}$ is relatively transparent. Distinct from stiff inorganic bulks on the one hand and completely soft polymer on the other hand, the well-balanced ductility and stiffness could reasonably ensure supporting scaffolds for applications within biomedical fields. To evaluate the size of SiO_2 and TiO_2 particles after sol-formation, we have performed

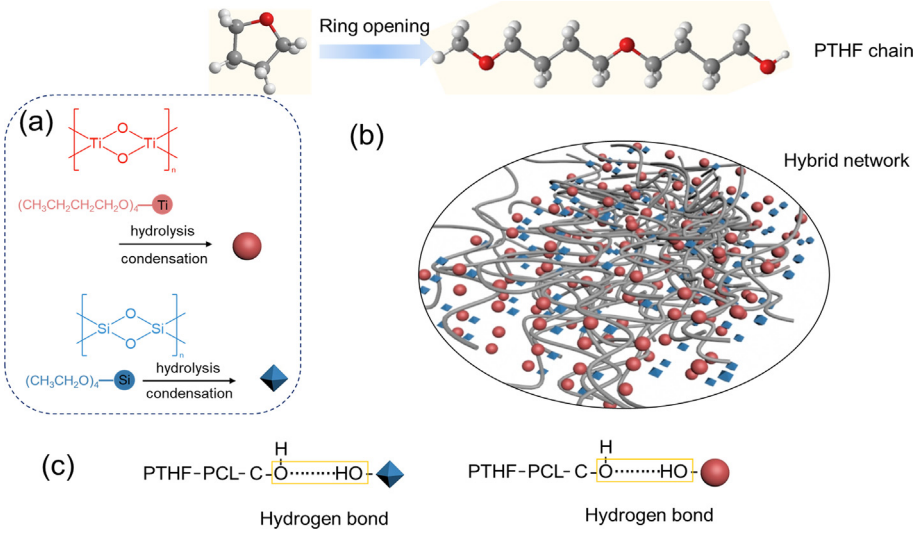

Fig. 1. Schematic illustration of the polymer–SiO_2/TiO_2 hybrid structure. (a) Hydrolysis and condensation processes of inorganic precursors; (b) structure of hybrids with the PTHF–PCL–COOH–SiO_2/TiO_2 network; (c) hydrogen bonds among inorganic particles and polymer chains.

DLS measurements using a Zetasizer Range [37,38] (Fig. 2b) before further reacting with the organic precursor of PCL–PTHF–GPTMS. The most typical size of SiO_2-sol was found to be 9 nm with a relatively narrow size distribution, whereas the size of TiO_2 was in a range of 10–20 nm with broader distribution. The nanoscale size of these components is beneficial for their uniformed reaction with every reactive terminal trimethoxysilane group of GPTMS–PTHF–PCL and thus controls the structure of the hybrids at the nanoscale [35]. Co-networks formed by inorganic composites and polymers could be formed during the long-time polycondensation process.

Then, for the prepared samples, the spatial distribution of inorganic particles and polymer chains can also be detected through element mapping by means of scanning electron microscopy–energy dispersive X-ray (SEM-EDX) analysis. As is shown in Fig. S3, the surface of the hybrid polymer$_{70}$/(Si$_{0.6}$Ti$_{0.4}$)$_{30}$ is relatively uniform. That is, the main elements C, O, Si, and Ti are all evenly distributed across the surface. Because polymer chains are the main component in the hybrids, C is easily detected. The analysis also shows that inorganic composites are well integrated in the hybrids. Furthermore, to determine the morphology and dispersion of SiO_2 and TiO_2 composites, we have performed TEM and HAADF-STEM analyses on the hybrids polymer$_{70}$/(Si$_0$Ti$_1$)$_{30}$, polymer$_{70}$/(Si$_1$Ti$_0$)$_{30}$, and polymer$_{70}$/(Si$_{0.6}$Ti$_{0.4}$)$_{30}$. As shown in Fig. 2c, the inorganic nanoparticles of SiO_2 and TiO_2 are irregular with a size of around 10–30 nm in the hybrid polymer$_{70}$/(Si$_{0.6}$Ti$_{0.4}$)$_{30}$. The elemental mapping images of Si, Ti, and C presented in Fig. 2d–f reveal that the inorganic components are homogeneously dispersed in the hybrid material, without aggregation of separate SiO_2 or TiO_2 clusters. The reason for this could be the Si–O–Ti bonds that are formed between these two inorganic composites as a result of the long-term sol–gel processes [35,39]. Moreover, the element mapping images of hybrid polymer$_{70}$/(Si$_0$Ti$_1$)$_{30}$ in Fig. S4a show that the size of TiO_2 nanoparticles is around 10 nm. The detection of small amounts of the Si element is ascribed to the coupling agent GPTMS, which functions as a bridge between polymer and inorganic composites. When TiO_2 dominates the hybrid polymer$_{70}$/(Si$_0$Ti$_1$)$_{30}$, TiO_2 could easily get agglomerated as shown in Fig. S4c. However, Si elements in the hybrid polymer$_{70}$/(Si$_1$Ti$_0$)$_{30}$ (see Fig. S5b) are uniformly dispersed in the hybrid material, without aggregation or apparent inorganic clusters. Thus, we infer that TiO_2 is covalently linked to the polymers by forming covalent bonds with SiO_2 during the sol–gel process. Excess TiO_2 nanoparticles might easily aggregate, whereas this is not the case for SiO_2 nanoparticles.

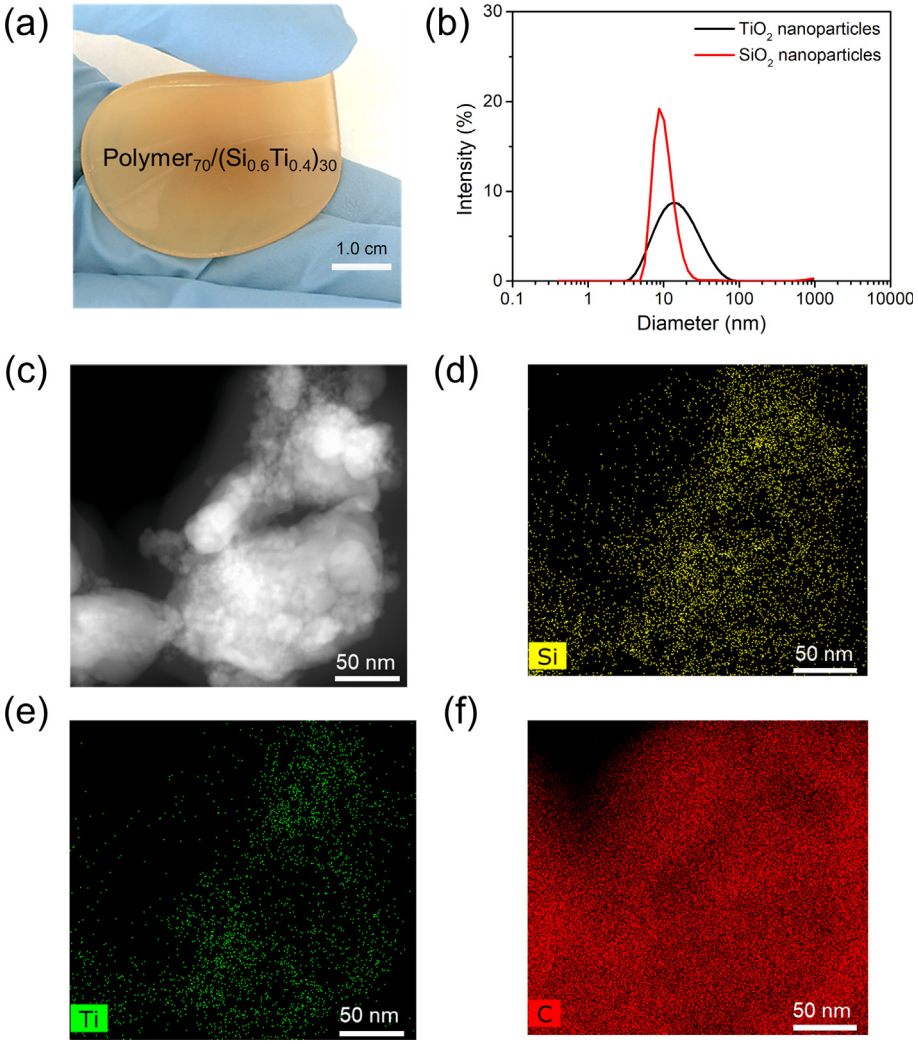

Fig. 2. (a) Image illustrating the flexibility of the hybrid polymer$_{70}$/(Si$_{0.6}$Ti$_{0.4}$)$_{30}$; (b) size distribution of SiO_2 and TiO_2 nanoparticles as tested by DLS; (c) the HAADF-STEM image of the bulk of the polymer$_{70}$/(Si$_{0.6}$Ti$_{0.4}$)$_{30}$ hybrid and STEM images with corresponding element distribution of (d) Si, (e) Ti, and (f) C.

Next, we have performed FTIR spectroscopy measurements to characterize the molecular structures of the different hybrids (Fig. 3a). The bands at 568 cm^{-1} and 1,090 cm^{-1} can be assigned to typical stretching vibration of Ti–O–Ti bonds and asymmetric stretching vibration of Si–O–Si bonds, respectively [40]. The intensity of these bands varies in the different hybrids as a result of the varying fraction of inorganic particles [40,41]. Notably, we further ascribe the weak band at 920 cm^{-1} to stretching vibration of Si–O–Ti bonds, thus providing evidence for covalent linkage of SiO_2 and TiO_2 inorganic particles during the condensation reactions [31]. Considering the organic polymer chains, the observed peaks could also be assigned to PCL and PTHF. That is, the bands at 2,900, 1,730, and 1,200 cm^{-1} could be assigned to the characteristic stretching of $-CH_2-$, C=O, and –C–O–C– groups, respectively [18]. We have also performed XRD analysis and confirmed the amorphous structure of the hybrids (Fig. 3b). As expected, all the synthesized hybrids are fully amorphous, without any sharp diffracted peaks caused by crystals. The non-crystalline state is formed mainly because of the hydrolysis and condensation process of inorganic precursors, but also due to the Si–O–Ti bonds formed during the sol–gel process [28,35]. In accordance with the EDX results, the reason for the inorganic particles being uniformly dispersed in the system can likely be ascribed to the following factors: (i) the SiO_2 and TiO_2 particles are covalently bonded to PTHF polymer chains via the coupling agent GPTMS, (ii) SiO_2 and TiO_2 particles are bonded with each other through condensation, and (iii) non-covalent interactions, e.g. hydrogen bonds are formed between PCL–COOH and TiO_2/SiO_2.

The thermal stability of the six hybrids has been evaluated via TGA, as shown in Fig. 3c. The hybrids with both silica and titania feature improved their thermal stability in comparison with those containing only one type of inorganic component. It could be seen from the first order derivative of weight loss (inset of Fig. 3c) that the decomposition temperature of all hybrids is very close, mainly because polymer components begin to degrade in that temperature range. We further analyzed them via differential scanning calorimetry (DSC) as presented in Fig. 3d. Small peaks at around 220 °C are observed for single inorganic particle–based hybrids (SIHs). However, the exothermic peak area (around 400 °C) of DIHs is much larger than that of SIHs, representing higher enthalpy of decomposition of the polymer degradation process for DIHs. Based on aforementioned findings, we conclude that the hierarchical dual inorganic-composite structure forms a compact structure and multiple interactions between polymers and inorganic components, which improve the thermal stability of the hybrids. Another possible reason is that O_2 diffusion is reduced because of the addition of dual inorganic particles [42], and hence, the thermo-oxidative degradation takes longer time at the interior of the

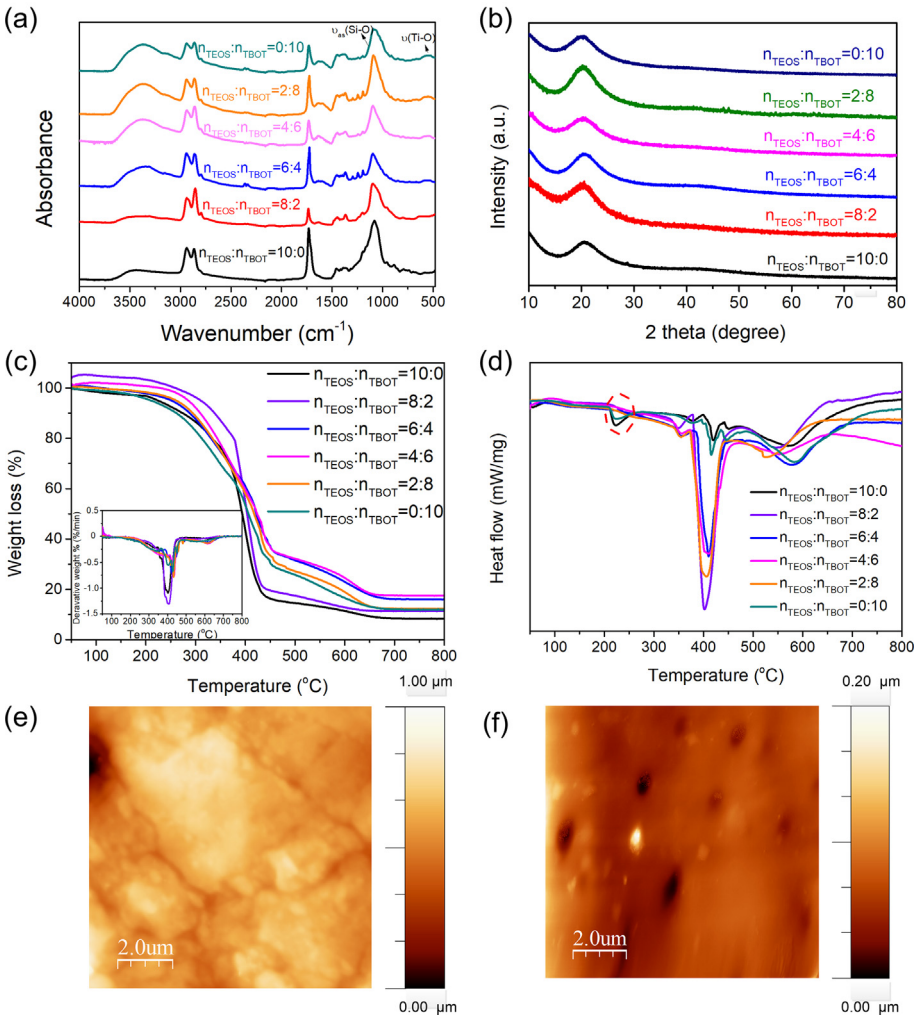

Fig. 3. Studies of (a) FT-IR, (b) XRD, (c) TGA, and (d) DSC on hybrids with different SiO_2/TiO_2 ratios (as reflected by the TEOS-to-TBOT ratio); (e, f) AFM topography phase images of hybrids polymer$_{70}$/$(Si_{0.6}Ti_{0.4})_{30}$ and polymer$_{70}$/$(Si_0Ti_1)_{30}$, respectively.

samples. Moreover, the bond energy of Si–C, Si–O, and Ti–O is 290, 432, and 662 kJ/mol, respectively [36], and therefore, the higher bond energy of Ti–O could also help to explain the observed behavior.

The actual total I/O weight ratios in the hybrids vary with composition, i.e. it firstly increases and then decreases with increasing titania content (Table 1). First, we note that TiO_2 could only bond to hybrid materials with SiO_2, and the amount of TiO_2 bonded to the hybrid networks is positively correlated with that of SiO_2. The molecular weight of TiO_2 is 76.87 g/mol, whereas that of SiO_2 is 60.08 g/mol. Thus, we believe that the I/O ratio increases slightly when the amount of SiO_2 dominates the hybrid. That is, all TiO_2 could bond with the hybrid and contributes to final I/O ratios. However, when TiO_2 becomes prevalent, the number of reactive sites is reduced simultaneously and excessive TiO_2 could not effectively bond to the hybrid. TiO_2 aggregates may thus form that are not connected to anything and likely washed away in the rinsing stage. The fact that TiO_2 is not as good a glass network former as SiO_2 might be another reason why less Ti is incorporated into the hybrids as the TEOS content decreases.

The morphology of the surface of the hybrids was further investigated through AFM analyses. Specifically, we have compared the topography and phase images of polymer$_{70}$/(Si$_{0.6}$Ti$_{0.4}$)$_{30}$ (Fig. 3e) and polymer$_{70}$/(Si$_0$Ti$_1$)$_{30}$ (Fig. 3f). In accordance with TEM and XRD results, components are dispersed uniformly and phase aggregation is avoided with the hybrid polymer$_{70}$/(Si$_{0.6}$Ti$_{0.4}$)$_{30}$ (Fig. S6). On the contrary, porous microstructures (black pores in Fig. 3f) and phase aggregations are observed in the hybrid polymer$_{70}$/(Si$_0$Ti$_1$)$_{30}$. This is likely due to the drying and aging process, after which the hybrids are washed with distilled water to remove by-products and non-covalently bonded inorganic particles. Thus, we believe that the micropores should be ascribed to the washed TiO_2 nanoparticles. It could also be observed that the cross-linking density of polymer$_{70}$/(Si$_{0.6}$Ti$_{0.4}$)$_{30}$ is much higher than that of the others (Fig. S7). Dual inorganic–based hybrids with multiple interactions among inorganic particles and polymer chains achieve uniformed dispersion of inorganic particles and largely enhance the cross-linking density and further contribute to mechanical enhancement of hybrids. SiO_2 and TiO_2 inorganic components bond together and form hybrid networks together with the hybrid polymer$_{70}$/(Si$_{0.6}$Ti$_{0.4}$)$_{30}$, whereas there will be fewer inorganic particles covalently bonded to polymer chains for the hybrid polymer$_{70}$/(Si$_0$Ti$_1$)$_{30}$. The results are also in accordance with the TGA analysis (Fig. 3c).

3.3. Mechanical tests of hybrids

Tensile [43] and compression tests [44] as well as DMA [45] were performed, aiming to understand the influence of the inorganic components on the mechanical response to identify the optimal hybrid composition and microstructure. The results are all recorded based on conventional strain and stress.

First, we consider the tensile test results in Fig. 4a. The DIHs with multimolecular interactions (covalent bonds, non-covalent interactions, physical cross-linking) generally possess higher strains at failure and ultimate tensile strengths than the SIHs. Among all the hybrids, the hybrid polymer$_{70}$/(Si$_{0.6}$Ti$_{0.4}$)$_{30}$ reveals the largest strain at failure of 39.2% and tensile strength of 68 kPa, whereas the hybrid polymer$_{70}$/(Si$_1$Ti$_0$)$_{30}$ exhibits the smallest ability to be stretched without fracturing ($\varepsilon_{f,T}$ = 4.8%), likely because the large fraction of the stiff and brittle silica network prevents plastic deformation during the stretching process. Nevertheless, the hybrid polymer$_{70}$/(Si$_0$Ti$_1$)$_{30}$ exhibits the lowest tensile strength (8.8 kPa). TiO_2 dominates in this system, and the decrease of total inorganic particles with fewer covalent bonds to polymer chains is the main reason for its low fracture strength.

Next, we consider DMA to obtain the storage modulus (E'), loss modulus (E''), and damping coefficient tan (δ) of the hybrids [46–50]. The storage and loss moduli represent the elastic and viscous portion, respectively, of the viscoelastic response of the hybrids. The change in the two moduli with the hybrid composition is depicted in Fig. 4b (for 1 Hz) and Fig. S8 (for 0.01–100 Hz). Results of E' and E'' of all hybrids at 1 Hz are summarized in Table S2. We observe that the storage modulus is almost ten times higher than the loss modulus for all six hybrids. Among the hybrids, all four DIHs reveal higher storage modulus than the two SIHs, among which polymer$_{70}$/(Si$_{0.6}$Ti$_{0.4}$)$_{30}$ exhibits the highest (160 kPa). Thus, stiffer hybrids are obtained through dual inorganic particle regulating. Moreover, the damping coefficient tan (δ), which is defined as the ratio of E'' to E', represents the relative contribution of the dissipative to elastic contribution and is considered as an indicator of how efficiently hybrids release energy to molecular rearrangement and internal friction [46,49,50] (Fig. S9). We note that the hybrid polymer$_{70}$/(Si$_{0.6}$Ti$_{0.4}$)$_{30}$ reveals relatively higher tan (δ) than other hybrids. This might be due to its higher cross-linking density and resulting stiffness. The internal frictions of polymer chains with SiO_2 restrain its elasticity and make it release energy more efficiently.

Finally, we also compared the mechanical properties of the hybrids via uniaxial compression tests of cylindrical monolith bulks. As is shown in Fig. 4c and S6, the representative stress–strain curves clearly illustrate that SiO_2-rich hybrids have higher compressive strength than TiO_2-rich ones. This suggests that the SiO_2 particles are easily covalently linked to the hybrid system compared with TiO_2 particles, and loss of inorganic particles reduces the compressive strength of TiO_2-rich hybrids. Of all the studied hybrids, polymer$_{70}$/(Si$_{0.6}$Ti$_{0.4}$)$_{30}$ features the best flexibility, as it could be compressed to a strain of 80% (at 1.4 MPa). For comparison, the conventional stress to failure of our prepared polymer$_{70}$/(Si$_{0.6}$Ti$_{0.4}$)$_{30}$ thus reaches 1.4 MPa, whereas the true stress to failure for the materials of Tallia et al. [18] is only 1.2 MPa, even though the inorganic composite content in their system is higher (24.7%) than that in ours (17.5%). The reason is due to its more compact structure and multistrengthening mechanism of dual inorganic particles. Thus, flexible DIHs are achieved by utilizing mixed SiO_2/TiO_2 as the multifunctional inorganic constituent of hybrids. The modulus of toughness of hybrids, which represents how much energy our prepared hybrids can absorb before rupturing, obtained as the total area under the stress–strain curve, is shown in Fig. 4d. It could be seen that DIHs maintain higher strength than SIHs, which indicates DIHs reveal the property of strength and ductility. Among the hybrids, polymer$_{70}$/(Si$_{0.6}$Ti$_{0.4}$)$_{30}$ has the highest modulus of toughness. The tangent modulus of the hybrids under certain strains is shown in Fig. S10 and Table S3 (strains at 20% can be compared). Polymer$_{70}$/(Si$_{0.4}$Ti$_{0.6}$)$_{30}$ and polymer$_{70}$/(Si$_{0.6}$Ti$_{0.4}$)$_{30}$ have low tangent modulus for a strain of 20%, namely, 0.21 and 0.59 MPa, respectively. Compared with other hybrids, polymer$_{70}$/(Si$_{0.4}$Ti$_{0.6}$)$_{30}$ and polymer$_{70}$/(Si$_{0.6}$Ti$_{0.4}$)$_{30}$ thus exhibit easier deformation. Tough materials are urgently needed in

Table 1
Actual values of I/O (wt%) as measured from TGA in the final hybrid samples.

Hybrid	I/O wt%
Polymer$_{70}$/(Si$_1$Ti$_0$)$_{30}$	11.9/88.1
Polymer$_{70}$/(Si$_{0.8}$Ti$_{0.2}$)$_{30}$	12.3/87.7
Polymer$_{70}$/(Si$_{0.6}$Ti$_{0.4}$)$_{30}$	17.5/82.5
Polymer$_{70}$/(Si$_{0.4}$Ti$_{0.6}$)$_{30}$	16.1/83.9
Polymer$_{70}$/(Si$_{0.2}$Ti$_{0.8}$)$_{30}$	11.3/88.7
Polymer$_{70}$/(Si$_0$Ti$_1$)$_{30}$	8.3/91.7

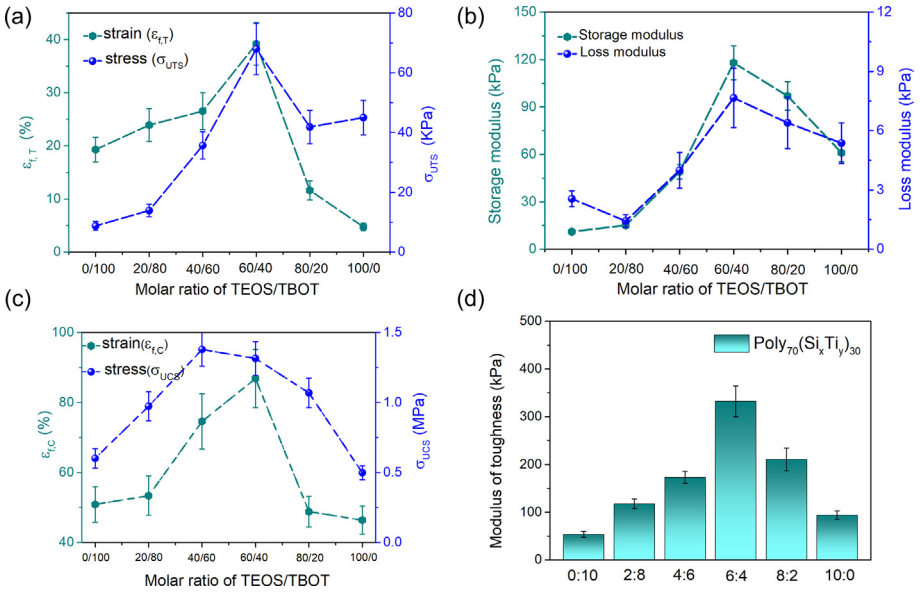

Fig. 4. Mechanical performance of the hybrids. (a) Composition dependence of ultimate tensile strength (σ_{UTS}) and tensile strain at failure ($\varepsilon_{f,T}$) as obtained from uniaxial tensile testing. (b) composition dependence of storage modulus (E') and loss modulus (E'') as obtained from DMA in compression at 1 Hz; (c) composition dependence of ultimate compressive strength (σ_{UCS}) and compressive strain at failure ($\varepsilon_{f,C}$) as obtained from compression testing; (d) modulus of toughness of hybrids with different SiO_2/TiO_2 compositions from the compression test.

many practical application fields such as tissue engineering and soft robotics, for example, native human articular cartilage has a compression modulus of about 0.4–2.0 MPa [51,52]. Our results show that the hybrid polymer$_{70}$/(Si$_{0.6}$Ti$_{0.4}$)$_{30}$ has the highest compressive ultimate strength (1.3 MPa), modulus of toughness (332 kPa), up to 37% tensile elongation, and compression modulus of 0.59 MPa, thus falling within the needed property range. Such an inorganic–polymer hybrid design with optimized mechanical properties therefore offers good prospects for future applications.

4. Conclusion

In summary, we have prepared flexible inorganic–organic hybrids by controlling the compositions of dual inorganic components. Covalent bonds in polymer–polymer, polymer–SiO_2 network, and TiO_2–SiO_2 inorganic particles as well as reversible intermolecular interactions (e.g. London forces and hydrogen bonds) all play important roles in synergistically promoting the improved fracture stress and strain in the mixed hybrid materials. The hybrid polymer$_{70}$/(Si$_{0.6}$Ti$_{0.4}$)$_{30}$ reveals optimal mechanical properties compared with the other hybrids. For the DIHs, the multiple interactions existing among polymer chains and inorganic components prevent the fracture propagation during the tensile deformation and compression processes, which reveals the potential in obtaining hybrids that can be deformed without fracture. This work refines the roles of different inorganic particles on the mechanical properties of organic–inorganic hybrid materials, and we believe such findings will be important for the design of ductile hybrids that can be applied in soft robotics and biomedical fields.

Credit author statement

W.F., M.M.S., and D.Y. conceived the study and designed the experiments. M.M.S. and D.Y. supervised the project. W.F. prepared the samples and performed the basic structure characterization. W.F. and L.R.J. performed the mechanical characterization. M.C. performed the TEM experiments. T.S.Q. performed the DMA experiments. L.G. performed the AFM experiments. W.F., M.M.S., and D.Y. wrote the manuscript with inputs from other co-authors. All authors contributed to analyzing and discussing the data.

Declaration of competing interest

The authors declare that they have no known competing financial interests or personal relationships that could have appeared to influence the work reported in this article.

Acknowledgments

This work was supported by the China Scholarship Council (CSC No. 201904910782).

Appendix A. Supplementary data

Supplementary data to this article can be found online at https://doi.org/10.1016/j.mtchem.2021.100584.

References

[1] Q. Fu, E. Saiz, M.N. Rahaman, A.P. Tomsia, Toward strong and tough glass and ceramic scaffolds for bone repair, Adv. Funct. Mater. 23 (2013) 5461–5476.
[2] L. Che, Z. Lei, P. Wu, D. Song, A 3D printable and bioactive hydrogel scaffold to treat traumatic brain injury, Adv. Funct. Mater. 29 (2019) 1904450.
[3] F. Baino, E. Fiume, M. Miola, E. Verné, Bioactive sol-gel glasses: processing, properties, and applications, Int. J. Appl. Ceram. Technol. 15 (2018) 841–860.
[4] J.R. Jones, Review of bioactive glass: from Hench to hybrids, Acta Biomater. 9 (2013) 4457–4486.
[5] G.J. Owens, R.K. Singh, F. Foroutan, M. Alqaysi, C.-M. Han, C. Mahapatra, H.-W. Kim, J.C. Knowles, Sol–gel based materials for biomedical applications, Prog. Mater. Sci. 77 (2016) 1–79.
[6] J.Y. Sun, X. Zhao, W.R. Illeperuma, O. Chaudhuri, K.H. Oh, D.J. Mooney, J.J. Vlassak, Z. Suo, Highly stretchable and tough hydrogels, Nature 489 (2012) 133–136.
[7] B.M. Novak, Hybrid nanocomposite materials? Between inorganic glasses and organic polymers, Adv. Mater. 5 (1993) 422–433.
[8] Y. Vueva, L.S. Connell, S. Chayanun, D. Wang, D.S. McPhail, F. Romer, J.V. Hanna, J.R. Jones, Silica/alginate hybrid biomaterials and assessment of their covalent coupling, Appl. Mater. Today 11 (2018) (2018) 1–12.
[9] O. Mahony, O. Tsigkou, C. Ionescu, C. Minelli, L. Ling, R. Hanly, M.E. Smith, M.M. Stevens, J.R. Jones, Silica-gelatin hybrids with tailorable degradation and mechanical properties for tissue regeneration, Adv. Funct. Mater. 20 (2010) 3835–3845.

[10] A. Kumar, K.M. Rao, S.S. Han, Synthesis of mechanically stiff and bioactive hybrid hydrogels for bone tissue engineering applications, Chem. Eng. J. 317 (2017) 119–131.
[11] J.J. Chung, S. Li, M.M. Stevens, T.K. GePolyiou, J.R. Jones, Tailoring mechanical properties of sol–gel hybrids for bone regeneration through polymer structure, Chem. Mater. 28 (2016) 6127–6135.
[12] L.S. Connell, L. Gabrielli, O. Mahony, L. Russo, L. Cipolla, J.R. Jones, Functionalizing natural polymers with alkoxysilane coupling agents: reacting 3-glycidoxypropyl trimethoxysilane with poly(γ-glutamic acid) and gelatin, Polym. Chem. 8 (2017) 1095–1103.
[13] E.M. Valliant, F. Romer, D. Wang, D.S. McPhail, M.E. Smith, J.V. Hanna, J.R. Jones, Bioactivity in silica/poly(gamma-glutamic acid) sol-gel hybrids through calcium chelation, Acta Biomater. 9 (2013) 7662–7671.
[14] L.L. Hench, I. Thompson, Twenty-first century challenges for biomaterials, J. R. Soc. Interface 7 (2010) S379–S391.
[15] U.G. Wegst, H. Bai, E. Saiz, A.P. Tomsia, R.O. Ritchie, Bioinspired structural materials, Nat. Mater. 14 (2015) 23–36.
[16] L.S. Connell, F. Romer, M. Suarez, E.M. Valliant, Z. Zhang, P.D. Lee, M.E. Smith, J.V. Hanna, J.R. Jones, Chemical characterisation and fabrication of chitosan-silica hybrid scaffolds with 3-glycidoxypropyl trimethoxysilane, J. Mater. Chem. B 2 (2014) (2014) 668–680.
[17] W. Fan, R.E. Youngman, X. Ren, D. Yu, M.M. Smedskjaer, J. Mater. Chem. B 9 (2021) 4400–4410.
[18] F. Tallia, L. Russo, S. Li, A.L.H. Orrin, X. Shi, S. Chen, J.A.M. Steele, S. Meille, J. Chevalier, P.D. Lee, M.M. Stevens, L. Cipolla, J.R. Jones, Bouncing and 3D printable hybrids with self-healing properties, Mater. Horiz 5 (2018) 849–860.
[19] L. Gabrielli, L. Connell, L. Russo, J. Jiménez-Barbero, F. Nicotra, L. Cipolla, J.R. Jones, Exploring GPTMS reactivity against simple nucleophiles: chemistry beyond hybrid materials fabrication, RSC Adv. 4 (2014) 1841–1848.
[20] F.K. Shi, X.P. Wang, R.H. Guo, M. Zhong, X.M. Xie, Highly stretchable and super tough nanocomposite physical hydrogels facilitated by the coupling of intermolecular hydrogen bonds and analogous chemical crosslinking of inorganic particles, J. Mater. Chem. B 3 (2015) 1187–1192.
[21] L.-q. Zhang, L.-w. Chen, M. Zhong, F.-k. Shi, X.-y. Liu, X.-m. Xie, Phase transition temperature controllable poly(acrylamide-co-acrylic acid) nanocomposite physical hydrogels with high strength, Chin. J. Polym. Sci. 34 (2016) 1261–1269.
[22] F.K. Shi, M. Zhong, L.Q. Zhang, X.Y. Liu, X.M. Xie, Robust and self-healable nanocomposite physical hydrogel facilitated by the synergy of ternary crosslinking points in a single network, J. Mater. Chem. B 4 (2016) 6221–6227.
[23] M. Zhong, X.Y. Liu, F.K. Shi, L.Q. Zhang, X.P. Wang, A.G. Cheetham, H. Cui, X.M. Xie, Self-healable, tough and highly stretchable ionic nanocomposite physical hydrogels, Soft Matter 11 (2015) (2015) 4235–4241.
[24] D. Wang, W. Liu, Q. Feng, C. Dong, Q. Liu, L. Duan, J. Huang, W. Zhu, Z. Li, J. Xiong, Y. Liang, J. Chen, R. Sun, L. Bian, D. Wang, Effect of inorganic/organic ratio and chemical coupling on the performance of porous silica/chitosan hybrid scaffolds, Mater. Sci. Eng. C 70 (2017) 969–975.
[25] M. Mokhtarifar, R. Kaveh, M. Bagherzadeh, A. Lucotti, M. Pedeferri, M.V. Diamanti, Heterostructured TiO_2/SiO_2/gamma-Fe_2O_3/rGO coating with highly efficient visible-light-induced self-cleaning properties for metallic artifacts, ACS Appl. Mater. Interfaces 12 (2020) 29671–29683.
[26] J. Hu, Q. Gao, L. Xu, M. Zhang, Z. Xing, X. Guo, K. Zhang, G. Wu, Significant improvement in thermal and UV resistances of UHMWPE fabric through in situ formation of polysiloxane-TiO_2 hybrid layers, ACS Appl. Mater. Interfaces 8 (2016) 23311–23320.
[27] P. Yu, R.J. Kirkpatrick, B. Poe, P.F. McMillan, X. Cong, Structure of calcium silicate hydrate (C-S-H): near-, mid-, and far-infrared spectroscopy, J. Am. Ceram. Soc. 82 (2004) 742–748.27.
[28] D. Wang, Y. Tan, L. Yu, Z. Xiao, J. Du, J. Ling, N. Li, J. Wang, S. Xu, J. Huang, Tuning morphology and mechanical property of polyacrylamide/laponite/titania dual nanocomposite hydrogels by titania, Polym. Compos. 40 (2019) (2019) E466–E475.
[29] L.L. Hench, J.K. West, The sol-gel process, Chem. Rev. 90 (1990) 33–72.
[30] D. Zhang, J. Yang, S. Bao, Q. Wu, Q. Wang, Semiconductor nanoparticle-based hydrogels prepared via self-initiated polymerization under sunlight, even visible light, Sci. Rep. 3 (2013) 1399.
[31] F.H. Aragón, I. Gonzalez, J.A.H. Coaquira, P. Hidalgo, H.F. Brito, J.D. Ardisson, W.A.A. Macedo, P.C. Morais, Structural and surface study of praseodymium-doped SnO_2 nanoparticles prepared by the polymeric precursor method, J. Phys. Chem. C 119 (2015) 8711–8717.
[32] F. Fan, Z. Xia, Q. Li, Z. Li, H. Chen, ZrO2/PMMA nanocomposites: preparation and its dispersion in polymer matrix, Chin. J. Chem. Eng. 21 (2013) 113–120.
[33] H. Li, C.P. Tripp, Infrared study of the interaction of charged silica particles with TiO_2 particles containing adsorbed cationic and anionic polyelectrolytes, Langmuir 21 (2005) 2585–2590.
[34] R. Peña-Alonso, L. Téllez, J. Rubio, F. Rubio, Surface chemical and physical properties of TEOS-TBOT-PDMS hybrid materials, J. Sol Gel Sci. Technol. 38 (2006) 133–145.
[35] J. Du, X. She, W. Zhu, Q. Yang, H. Zhang, C. Tsou, Super-tough, anti-fatigue, self-healable, anti-fogging, and UV shielding hybrid hydrogel prepared via simultaneous dual in situ sol-gel technique and radical polymerization, J. Mater. Chem. B 7 (2019) 7162–7175.
[36] R.T. Sanderson, Chemical Bonds and Bond Energy, second ed., 1976.
[37] M. Lehmann, W. Tabaka, T. Moller, A. Oppermann, D. Woll, D. Volodkin, S. Wellert, R.V. Klitzing, DLS setup for in situ measurements of photoinduced size changes of microgel-based hybrid particles, Langmuir 34 (2018) 3597–3603.
[38] S. Bhattacharjee, DLS and zeta potential – what they are and what they are not? J. Controlled Release 235 (2016) 337–351.
[39] M. Liu, Y. Qing, Y. Wu, J. Liang, S. Luo, Facile fabrication of superhydrophobic surfaces on wood substrates via a one-step hydrothermal process, Appl. Surf. Sci. 330 (2015) 332–338.
[40] F. Rubio, J. Rubio, J.L. Oteo, A FT-IR study of the hydrolysis of tetraethylorthosilicate (TEOS), Spectrosc. Lett. 31 (1998) 199–219.
[41] E. Norris, C. Ramos-Rivera, G. Poologasundarampillai, J.P. Clark, Q. Ju, A. Obata, J.V. Hanna, T. Kasuga, C.A. Mitchell, G. Jell, J.R. Jones, Electrospinning 3D bioactive glasses for wound healing, Biomed. Mater. 15 (2020), 015014.
[42] K. Chrissafis, D. Bikiaris, Can nanoparticles really enhance thermal stability of polymers? Part I: an overview on thermal decomposition of addition polymers, Thermochim. Acta 523 (2011) 1–24.
[43] W. Wu, Q. Wang, W. Li, Comparison of tensile and compressive properties of carbon/glass interlayer and intralayer hybrid composites, Materials 11 (2018) 1105.
[44] G. Czél, M. Jalalvand, M.R. Wisnom, Hybrid specimens eliminating stress concentrations in tensile and compressive testing of unidirectional composites, Compos. A 91 (2016) 436–447.
[45] S.C. Her, K.Y. Lin, Dynamic mechanical analysis of carbon nanotube-reinforced nanocomposites, J. Appl. Biomater. Funct. Mater. 15 (2017) e13–e18.
[46] C.S.M.F. Costa, A.C. Fonseca, A.C. Serra, J.F.J. Coelho, Dynamic mechanical thermal analysis of polymer composites reinforced with natural fibers, Polym. Rev. 56 (2016) 362–383.
[47] L. Chen, X. Zhang, G. Liu, Analysis of dynamic mechanical properties of sprayed fiber-reinforced concrete based on the energy conversion principle, Constr. Build. Mater. 254 (2020) 119167.
[48] K.V. Pillai, S. Renneckar, Dynamic mechanical analysis of layer-by-layer cellulose nanocomposites, Ind. Crops Prod. 93 (2016) 267–275.
[49] Z. Deng, X. Liu, X. Yang, N. Liang, R. Yan, P. Chen, Q. Miao, Y. Xu, A study of tensile and compressive properties of hybrid basalt-polypropylene fiber-reinforced concrete under uniaxial loads, Struct. Concr. 22 (2020) 396–409.
[50] M.S. Islam, S. Hamdan, Z.A. Talib, A.S. Ahmed, M.R. Rahman, Tropical wood polymer nanocomposite (WPNC): the impact of nanoclay on dynamic mechanical thermal properties, Compos. Sci. Technol. 72 (2012) 1995–2001.
[51] W. Zhao, X. Jin, Y. Cong, Y. Liu, J. Fu, Degradable natural polymer hydrogels for articular cartilage tissue engineering, J. Chem. Technol. Biotechnol. 88 (2013) 327–339.
[52] L.A. Setton, D.M. Elliott, V.C. Mow, Altered mechanics of cartilage with osteoarthritis: human osteoarthritis and an experimental model of joint degeneration, Osteoarthr. Cartil. 7 (1999) 2–14.